International Journal of Greenhouse Gas Control 86 (2019) 82–92

Contents lists available at ScienceDirect

International Journal of Greenhouse Gas Control

journal homepage: www.elsevier.com/locate/ijggc

Reactive transport modelling insights into CO_2 migration through sub-vertical fluid flow structures

H. Marín-Moreno[a,*], Jonathan M. Bull[b], Juerg M. Matter[b], David J. Sanderson[b], Ben J. Roche[b]

[a] National Oceanography Centre, University of Southampton Waterfront Campus, European Way, Southampton, SO14 3ZH, United Kingdom
[b] Ocean and Earth Science, University of Southampton, European Way, Southampton, SO14 3ZH, United Kingdom

ARTICLE INFO

Keywords:
Marine environment
CO_2 leakage
Chimney
Fractures
Numerical modelling
Reactive transport

ABSTRACT

Sub-vertical geological structures that cut through the overburden, usually called chimneys or pipes, are common in sedimentary basins. Chimneys behave as conduits that hydraulically connect deep strata with the overburden and seabed. Hence, if stored CO_2 migrates to a sufficiently high permeability chimney the risk of CO_2 leakage at the seabed increases. Despite the possible negative effects these structures may have on the integrity of CO_2 storage sites, little is known about (i) their effective permeability distribution, controlled by the combined role of fractures and matrix, and (ii) feedback mechanisms between porosity-permeability, CO_2 reactivity and mineralogy within them. Reactive transport modelling is used to perform 2D axisymmetric radial simulations of geological systems containing chimneys. CO_2 saturations of 10%, 30% and 50% are imposed on a cell located next to the symmetry axis at the base of the model. Under hydrostatic conditions, CO_2 reaches the seabed, at 500 m above the injection point, in less than 100 yr using injected CO_2 saturations at or above 30% and with overburden isotropic permeabilities and chimney vertical permeabilities above 10^{-14} m^2. Vertical fractures with apertures larger than 0.05 mm for volume fractions below 1% are sufficient to sustain such high vertical permeabilities in the chimney with a relatively high cap rock matrix permeability of 10^{-16} m^2. Over 100 yr of CO_2 injection, changes in porosity and permeability due to mineral precipitation/dissolution are negligible. For this time scale, in systems containing chimneys sufficiently far away from the injection well, the risk of CO_2 leakage at the seabed is primarily controlled by the pre-existing hydrogeological state of the system.

1. Introduction

A major concern in the storage of CO_2 in geological reservoirs is avoiding leakage of sequestered CO_2 into the water column or into the atmosphere. Potential pathways for CO_2 leakage may include CO_2 injection pressure-induced fractures (e.g., Rutqvist et al., 2008), micro-fractures caused by a rapid removal of grounded ice (Cavanagh and Haszeldine, 2014), and pre-existing sub-vertical conduits commonly named as chimneys, likely formed by fluid overpressure-induced capillary or fracture failure of the cap rock (e.g., Cartwright et al., 2007; Løseth et al., 2009; type-A anomaly according to Karstens and Berndt, 2015). These conduits are observed globally in passive continental margins (e.g., Berndt, 2005) and sedimentary basins offshore (e.g., Cartwright and Santamarina, 2015) and onshore (e.g., Dentzer et al., 2018). They can hydraulically connect the reservoir with the sediments above, sometimes even reaching the seabed/surface, and facilitate the upwards migration of pore fluids from deep stratigraphic layers (e.g., Karstens and Berndt, 2015). Offshore, they appear as sub-vertical anomalies and blanking in seismic data and are often found below seabed depressions or pockmarks (e.g., Hustoft et al., 2010).

The activity and geometry of chimney structures may be related: blowout-like isolated events likely result in columnar structures (e.g., Bünz et al., 2003; type-A anomaly according to Karstens and Berndt, 2015), while continuous long-lasting events form less well-defined sub-vertical structures (e.g., Arntsen et al., 2007; type-B anomaly according to Karstens and Berndt, 2015). In this work we focus on the former type of offshore chimneys but we do not investigate the hydromechanical coupling involved in their development.

Chimneys are associated with CO_2 storage sites such as Sleipner, North Sea (e.g., Chadwick et al., 2005) and Snøhvit, Barents Sea (e.g., Tasianas et al., 2016), but CO_2 seabed leakage has not been observed. Chimneys can be active with significant gas, mostly methane, emanating from the seabed. One example is the Scanner Pockmark Complex, located in the south of the UK license block 15/25, approximately 185 km off the north-east coast of Scotland (58°16′54.0″N, 0°58′14.6″E; Gafeira and Long, 2015). Further evidence supporting their active role

* Corresponding author.
E-mail address: hector.marin.moreno@noc.ac.uk (H. Marín-Moreno).

https://doi.org/10.1016/j.ijggc.2019.04.018
Received 25 October 2018; Received in revised form 15 March 2019; Accepted 25 April 2019

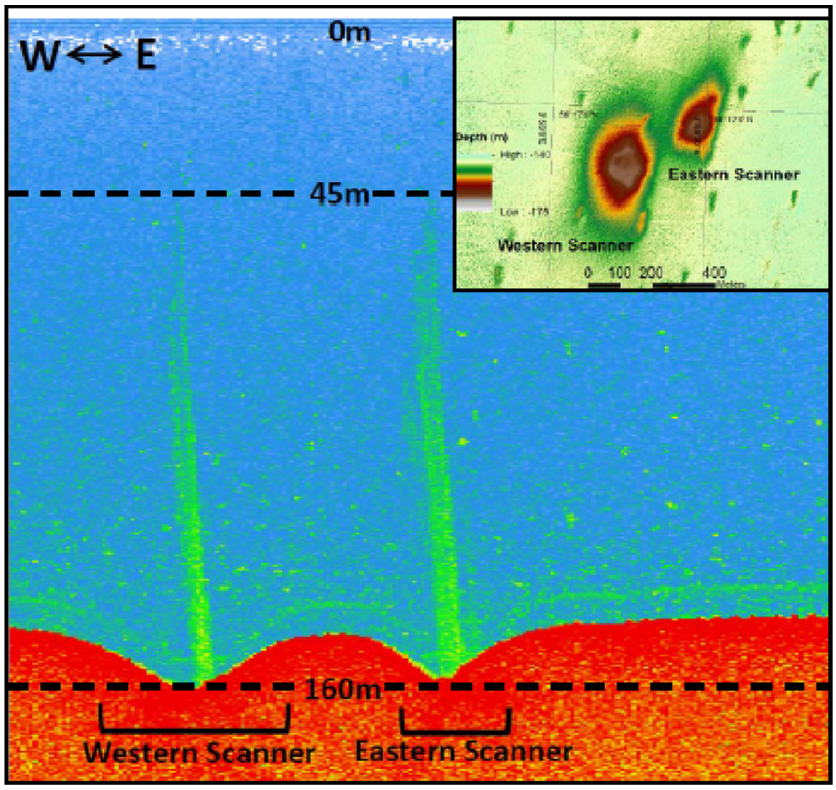

Fig. 1. Active methane venting imaged within the water column at the Scanner pockmark complex, North Sea. The bright flares observed in the multibeam echosounder (EM712) profile are caused by methane gas bubbles which rise from the seabed at 160 m to 40 m water depth before dissolving. The inset shows the morphology of the pockmarks. All data collected during James Cook 152 cruise in August 2017 (Bull et al., 2018a,b).

in this area comes from data acquired on-board RSS James Cook, expedition JC152 between 24th August and 13th of September 2017 (Fig. 1; Bull et al., 2018a,b).

The response of sub-seabed geological systems containing chimneys to the transport of CO_2 will depend on many factors including: geometry and size of the chimneys; porosity and permeability of the host sediment; aperture, separation, length, connectivity, and degree of sealing of the fractures within the chimneys; the physico-chemical properties of the brine; and the mineralogy of the background sediment. It is clear that a significant amount of detailed in-situ high resolution geophysical, geological and chemical data, in combination with laboratory experiments using samples from relevant sites, are needed to properly constrain the inputs and so outputs of reactive transport simulations. However, valuable insights on the system's response can still be gained by simulating scenarios that use relatively simplified and general geological models utilizing existing relevant data; this is our approach here. We use numerical simulation of the relevant flows and transport processes, and chemical reactions to explore the behavior of geological systems containing chimneys to changes in hydrogeological parameters.

We employ the reactive transport code TOUGHREACT V3.32 (Xu et al., 2017) complemented with the fluid property module ECO2N (Pruess, 2005) and a thermodynamic database adapted from the EQ3/6 geochemical modelling code (Wolery, 1992). Published work uses reactive transport simulation of CO_2 injection offshore in areas such as the United States Gulf Coast (e.g., Xu et al., 2003) or the Sleipner reservoir, North Sea (e.g., Audigane et al., 2007) to understand the processes and parameters governing the storage potential of such reservoirs. Our focus is different. The potential negative effects chimneys can have if a plume of stored CO_2 reaches them motivates this work. Here we assess the degree to which CO_2 fluxes from geological systems containing dormant well-defined columnar chimneys is controlled by their permeability distribution, or the combined role of fractures and matrix permeabilities, and feedback mechanisms between porosity-permeability and CO_2 reactivity and mineralogy within them.

2. Modelling approach

2.1. Major processes modelled and solution method

TOUGHREACT V3.32 is a code for the simulation of coupled subsurface multiphase fluid and heat flow, solute transport and chemical reactions in fracture and porous media. Here we describe the most important physical processes we model and summarize the numerical solution method; more detailed information is available from the TOUGHREACT V3 and ECO2N online manuals (see acknowledgements for the online links to these manuals).

The major fluid and heat flow processes considered are: (i) multiphase fluid flow (H_2O and CO_2) driven by pressure, viscous and gravity forces; (ii) partitioning of H_2O and CO_2 between liquid and gas phases; (iii) interactions between fluid phases governed by relative permeability and capillary pressure relationships; (iv) heat transfer by conduction and convection; (v) dependence of thermophysical properties (viscosity, density, and specific enthalpy) and solubility of H_2O (in gas phase) and CO_2 (in liquid phase) on pressure, temperature, and composition of fluid phases. We only solve the thermal problem during the initialization process to obtain a thermal structure that is consistent with our assumed geothermal gradient. During the CO_2 injection simulations we consider isothermal conditions. Non-isothermal effects might be significant if the temperature of the injected CO_2 is different from that in the reservoir (Pruess and Müller, 2009). Hence, here we assume that the injection point at the well is sufficiently far away from the chimney (in both the lateral and vertical directions) that, even if the CO_2 was injected at a different temperature from that in the reservoir, when the CO_2 reaches the chimney its temperature is in equilibrium with the background regional temperature.

We consider transport of liquid and gaseous species by advection in both liquid and gas phases and chemical reactions including: (i) aqueous complexation, acid-base, redox, gas dissolution/exsolution and cation exchange under local equilibrium conditions and (ii) mineral dissolution/precipitation under either local equilibrium or kinetic conditions. We do not consider transport of CO_2 by multiphase

molecular diffusion because, for the temporal (100 yr) and spatial (W x H, 1000 m x 500 m) scales of our problem, its contribution to the total seabed CO_2 leakage is likely to be small compared to that from CO_2 gravity and/or pressure driven transport in gas phase or from advection of dissolved CO_2 in liquid phase (e.g., Ahmad et al., 2016; Audigane et al., 2007). Note that hydrodynamic dispersion, which can develop from sub-grid scale heterogeneities and create differences in fluid velocity in different pathways, is not explicitly implemented in TOUGHREACT V3.32, and hence not considered here. Feedback between changes in mineral dissolution/precipitation and changes in porosity and so permeability is implemented by calculating changes in mineral volume fractions.

TOUGHREACT V3.32 discretizes the continuous multiphase fluid and heat flow and transport equations into a system of coupled non-linear algebraic equations using the integral finite difference method (IFD; Narasimhan and Witherspoon, 1976) and an implicit time scheme, which is then solved by Newton-Raphson iteration. After the solution of the flow equations, the resulting fluid velocities, phase saturations and temperatures are used to solve the solute transport of total dissolved components and transport of gaseous species in a component-by-component basis. The resulting concentrations obtained by solving the transport equations are then introduced into the chemical reaction model to solve the system of mixed equilibrium-kinetic chemical reactions on a grid-block by grid-block basis by Newton-Raphson iteration only once (non-sequential iteration approach, SNIA; e.g., Xu et al., 1999).

2.2. Conceptual framework

We use a two-dimensional (2-D) axisymmetric radial model and a proxy for the pressure, temperature, geological, mineral and chemical conditions from the North Sea to assess the temporal evolution and spatial distribution of CO_2 within and outside chimneys. The North Sea is one the best studied areas for offshore CO_2 injection activities and provides good constraints to justify key input parameters and modelling assumptions. As explained above, CO_2 injection activities in the North Sea occur in reservoirs associated with chimneys (e.g., Chadwick et al., 2005) and this provides a strong context for the work presented here.

The geological model extends 500 m down from the seabed and is 1000 m wide, and comprises five lithological layers (Table 1). The numerical model uses a fine mesh with a total of 9432 elements and 18,661 connections in the radial and vertical directions, to achieve good spatial resolution and limit discretization error. The grid is finer in the zone surrounding the chimney (left boundary) and becomes increasingly coarser towards the right boundary. In the vertical direction, the grid is finer in the zone close to the injection point in the chimney (bottom left boundary), becomes coarser towards the middle of the model, and finer again towards the top boundary/seabed (Supplementary material Fig. S1).

Table 1
Initial sediment-dependent modelling parameters (solid grain density of 2600 kg m^3 was used for all sediments).

	WGF	CPF	LBF	AGF	NG
	Overburden				Cap rock
Top[a] [mbsf]	0	23	60	80	380
Bottom[a] [mbsf]	23	60	80	380	500
Porosity[b,c], ∅	0.4	0.3	0.3	0.3	0.1
Isotropic matrix permeability*, $k_{m,x} = k_{m,z}$ [m^2]	10^{-13} 10^{-14}	10^{-13} 10^{-14}	10^{-13} 10^{-14}	10^{-13} 10^{-14}	10^{-16}

WGF, Witch Ground Formation; CPF, Coal Pit Formation; LBF, Ling Bank Formation; AGF, Aberdeen Ground Formation; NG, Nordland Group.

[a] Judd et al. (1994).

[b] Paul and Jobson (1991) for WGF, CPF, LBF and AGF.

[c] Audigane et al. (2007) for NG.

* Note that we test two matrix permeabilities for the sediment layers comprising the overburden.

Table 2
Non sediment-dependent modelling parameters and applied relationships.

Parameter	Value	Reference
Seabed temperature [°C]	7	Shell UK Limited (2014)
Water depth [m]	165	Gafeira and Long (2015)
Initial salinity [wt %]	3.5	
Geothermal gradient [°C km^{-1}]	30	Harper (1971)
CO_2 saturation injection [%]	10, 30, 50	
CO_2 injection time [yr]	100	
"Tube in series" porosity-permeability model	$\frac{k_m}{k_{m0}} = \theta^2 \frac{1-\Gamma+\Gamma/\omega^2}{1-\Gamma+\Gamma(\theta/(\theta+\omega-1))^2}$; $\theta = \frac{1-S_s-\varnothing_r}{1-\varnothing_r}$; $\omega = 1+\frac{1/\Gamma}{1/\varnothing_r-1}$; $\varnothing_r = \Gamma = 0.8$	Verma and Pruess (1988)
Liquid relative permeability[a]	$k_{rl} = \sqrt{S^*}(1-(1-[S^*]^{1/m})^m)^2$; $S^* = (S_l - S_{lr})/(1-S_{lr})$; $S_{lr} = 0.2$; $m = 0.4$	van Genuchten (1980)
Gas relative permeability[a]	$k_{rg} = (1-\hat{S})^2(1-\hat{S}^2)$; $\hat{S} = (S_l - S_{lr})/(1-S_{lr}-S_{gc})$; $S_{lr} = 0.2$; $S_{gc} = 0.05$	Corey (1954)
Capillary pressure [Pa][a]	$P_{cap} = -P_0([S^*]^{-1/m}-1)^{1-m}$; $S^* = (S_l - S_{lr})/(1-S_{lr})$; $P_0 = 12500\,Pa$; $S_{lr} = 0.18$; $m = 0.4$	van Genuchten (1980)

k_m and k_{m0}, actual and initial permeabilities; Γ, fractional length of pore bodies; $\varnothing_r$, fraction of original porosity at which permeability goes to zero; S_s, fraction of the original pore space that is occupied by solids; $S_{(l,g)}$, liquid (l) and gas (g) saturation; S^* and $\hat{S}$, effective saturations; S_{lr}, residual liquid (l) saturation; S_{gc}, critical (g) saturation; m, exponent in the capillary pressure and relative permeability models; P_0, gas entry pressure.

[a] Assumed parameter values based on similar CO_2 injection studies (e.g., Pruess and Müller, 2009; Xu et al., 2011; Williams et al., 2018). Note that the values are the same for the cap rock and overburden, as also assumed in other related studies (e.g., Audigane et al., 2007; Mbia et al., 2014).

We fix the seabed (top boundary) temperature to an average annual seabed temperature of 7 °C (Shell UK Limited, 2014) and seabed pressure to 1.62 MPa, which corresponds to a water depth of about 165 m (Gafeira and Long, 2015) (Table 2). We also fix the temperature, pressure, mineralogy and concentration of dissolved components in water at the right boundary to those found regionally, because this boundary is sufficiently far away and insensitive to the CO_2 injection zone in the chimney. A zero flow condition is imposed on the bottom and left (symmetry axis) boundaries. The model was initialized to hydrostatic pressure conditions, assuming fully water saturated pores with 3.5% salinity, and to a constant geothermal gradient of 30 °C km^{-1} (Harper, 1971) by performing an initial fluid and heat flow simulation. The resulting pressure and temperature conditions (Supplementary material Fig. S2) where then used as initial conditions in the isothermal CO_2 injection simulations.

Our problem is conceptually similar to the injection of CO_2 into a reservoir with the major difference being that, instead of having a well connected to the sediment at the injection point only, we have a fully connected vertical structure. Hence, we adopt a common modelling strategy from CO_2 injection simulations in 2-D, and consider the left boundary as the axisymmetric axis coinciding with the centre of the chimney axis (Fig. 2; e.g., Williams et al., 2018). Another difference is that we fix the CO_2 gas saturation, on a grid block (0.5 m high and 0.5 m wide) located within the chimney and next to the symmetry axis at the base of the model, instead of directly fixing a CO_2 flux over the whole duration of the simulations of 100 yr. CO_2 gas saturations within a chimney can be derived from velocity analysis of seismic data (e.g.,

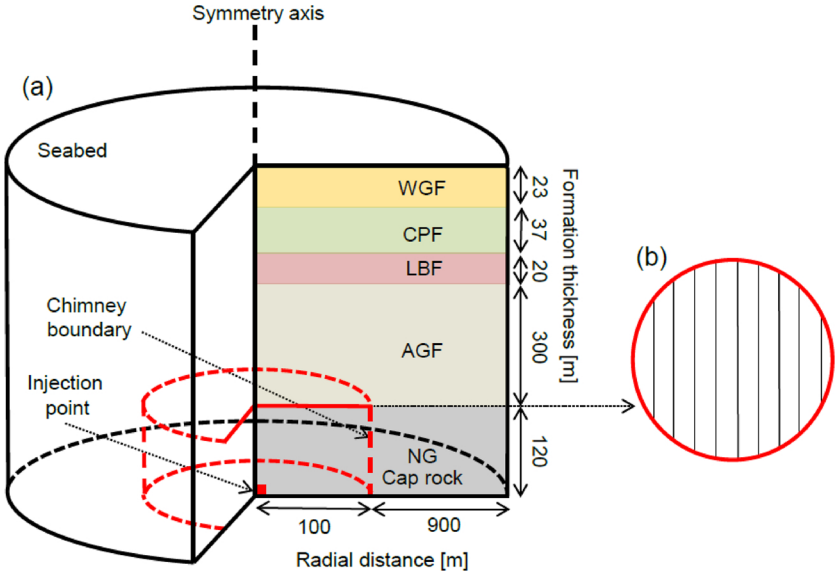

Fig. 2. (a) Schematic representation of our axisymmetric radial 2-D model used for simulation of sub-seabed CO_2 reactive transport through a chimney structure at the Scanner Pockmark Complex. (b) Schematic representation of the plan view of a section cutting through the chimney illustrating the conceptual model assumed in our simulations of a constant fracture density within a chimney for an assumed azimuthal orientation of fractures. Note that it is assumed that the chimney terminates at the top of the cap rock, NG formation. WGF, Witch Ground Formation; CPF, Coal Pit Formation; LBF, Ling Bank Formation; AGF, Aberdeen Ground Formation; NG, Nordland Group.

Chadwick et al., 2005). In contrast, estimating the flux at which the CO_2 migrates through a chimney is challenging and, indeed, one of the aims of this work. Note that the depth of the bottom boundary of the model is arbitrary and therefore our modelling represents part of a chimney. Hence, by fixing the CO_2 gas saturation, we essentially assume a constant flux of CO_2 reaching a depth of 120 m below the top of the chimney. The flux generated by imposing the CO_2 saturation mainly depends on the saturation value and the permeability of the chimney.

We assume a 100 m wide chimney (based on Karstens et al., 2017) and test CO_2 gas saturations of 10%, 30% and 50%. These CO_2 saturations are consistent with simulation results from CO_2 injection sites such as Sleipner, North Sea (e.g., Chadwick and Noy, 2015) or In Salah, Algeria (Preisig and Prévost, 2011) showing that high CO_2 saturations above 30% can reach distances of a few hundreds of meters from the injection well some years after injection starts.

We do not have in-situ constraints for the matrix permeabilities of the five sediment layers in our model, or the effective permeability of the chimney, governed by the combined role of fracture and matrix permeabilities. For the lithologies (Judd et al., 1994) and porosities (Paul and Jobson, 1991) of the four layers comprising the overburden we assume two matrix permeabilities of 10^{-14} m^2 and 10^{-13} m^2. Cap rocks typically have matrix permeabilities ranging from 10^{-16} to 10^{-19} m^2 in the absence of fractures (IEAGHG, 2011), but lower values from 10^{-21} to 10^{-19} m^2 are reported at relevant CO_2 storage sites (Espinoza and Santamarina, 2017). Cap rock permeabilities ranging from 10^{-20} to 10^{-14} m^2 have been used in CO_2 injection modelling studies in the North Sea (e.g., Audigane et al., 2007; Mbia et al., 2014; Williams et al., 2018) and of 10^{-16} m^2 in synthetic cases (e.g., Vilarrasa et al., 2010). We consider a relatively high cap rock isotropic matrix permeability of 10^{-16} m^2.

We consider that the chimney terminates at the top of the cap rock and contains closely spaced pre-existing sub-vertical fractures that mainly contribute to the flow on the direction they are aligned with (Fig. 2). In the chimney, based on this latter consideration, the fluid flow contribution from both fracture and porous flows can be approximated by the fluid flow of an equivalent homogenous media with effective horizontal and vertical permeabilities estimated from those of the individual components (fractures and pores). We use effective horizontal and vertical permeabilities ranging from 10^{-16} m^2 to 10^{-11} m^2. For simplicity, in this work we omit the term effective to refer to the permeability of the chimney. A summary of our major fluid flow related assumptions, and their justification and evaluation is presented in Appendix A, Table A1.

We use the relative permeability models proposed by van Genuchten (1980) for liquid and of Corey (1954) for gas, and van Genuchten's (1980) expression for capillary pressure. We note that we have changed the term residual gas saturation in Corey's (1954) model, as defined in TOUGHREACT v3.32, to critical gas saturation (CO_2 saturation above which CO_2 becomes mobile; below this value the relative permeability of CO_2 is zero). Changes in permeability caused by changes in porosity are calculated from the "tubes in series" model of Verma and Pruess (1988) (Table 2). We consider two different mineral assemblages (Table 3) and the chemical composition of typical seawater for the formation water (Table 4). For the Norland Group (the cap rock), we use the mineralogy from Audigane et al. (2007). For the layers above the Nordland Group (the overburden), we use the mineralogy of the Aberdeen Ground Formation (Stoker and Bent, 1987), which comprises 79% of the overburden thickness.

3. Results

A total of 46 simulations were performed using different combinations of permeability distributions within the chimney, overburden permeabilities, and CO_2 gas saturations injected (Fig. 3; Supplementary material Table T1). Injected CO_2 fluxes for the range of chimney permeabilities considered vary from 0.1 to 2 kg m^{-2} day^{-1}, from 2 to 350 kg m^{-2} day^{-1}, and from 9 to 4.5×10^3 kg m^{-2} day^{-1} for CO_2 saturations at the injection point of 10%, 30% and 50%, respectively. The associated CO_2 injection rates vary from 0.3 to 1.6×10^3 T yr^{-1}, which are orders of magnitude lower than typical well CO_2 injection rates of about a million tonnes per year. This is consistent with our assumption of the modelled chimney being located some distance away (several hundred meters to a few kilometers) from a hypothetical injection well. Under hydrostatic conditions, CO_2 reaches the seabed in less than 100 yr using injected CO_2 saturations at or above 30%, a critical gas saturation of 5%, and chimney vertical permeabilities and overburden isotropic permeabilities both above 10^{-14} m^2 (Fig. 3a, d). The resulting CO_2 fluxes at the seabed vary from 0.1 to 2 kg m^{-2} day^{-1}, similar to CO_2 natural leakage rates from 0.01 to 18 kg m^{-2} day^{-1} calculated from a range of leakage pathways globally (IEAGHG, 2011; the two most extreme values reported in that document have not been considered in the range). The simulation that considers a CO_2 saturation of 50% and a chimney vertical permeability of 10^{-11} m^2 gives the highest injected CO_2 flux of 4.5×10^3 kg m^{-2} day^{-1} and the highest CO_2 leakage at the seabed of 2 kg m^{-2} day^{-1} that starts just a few years after injection starts (Fig. 3a). For this simulation, only 0.04% of the

Table 3
Initial mineral volume fractions of considered mineral phases in two zones (Z1 and Z2) and their kinetic properties.

Mineral	Volume of solid [%]		A[c] [$cm^2\,g^{-1}$]	Parameters for kinetic rate law[c]							
				Neutral mechanism		Acid mechanism			Base mechanism		
	Z1[a]	Z2[b]		k_{25} [mol $m^{-2}\,s^{-1}$]	E_a [kJ mol^{-1}]	k_{25}	E_a	n(H)	k_{25}	E_a	n(OH)
Albite-low		13.20	9.8	$2.75E^{-13}$	69.8	$6.92E^{-11}$	65	0.457	$2.51E^{-16}$	71	−0.57
Ankerite			9.8	$1.26E^{-9}$	62.76	$6.46E^{-4}$	36.1	0.5			
Calcite	12.44	1.0	Assumed at local equilibrium								
Chalcedony		33.40	9.8	$1.02E^{-14}$	87.7						
Chlorite	6.22	4.40	9.8	$3.02E^{-13}$	88	$7.76E^{-12}$	88	0.5			
Dawsonite			9.8	$1.26E^{-9}$	62.76	$6.46E^{-4}$	36.1	0.5			
Dolomite			9.8	$2.95E^{-8}$	52.2	$6.46E^{-4}$	36.1	0.5			
Feldspar-K	15.79	2.30	9.8	$3.89E^{-13}$	38	$8.71E^{-11}$	51.7	0.5	$6.31E^{-12}$	94.1	−0.82
Hematite			12.9	$2.51E^{-15}$	66.2	$4.07E^{-10}$	66.2	1			
Illite	40.19		151.6	$1.66E^{-13}$	35	$1.05E^{-11}$	23.6	0.34	$3.02E^{-17}$	58.9	−0.4
Kaolinite	6.22	19.50	151.6	$6.92E^{-14}$	22.2	$4.90E^{-12}$	65.9	0.777	$8.91E^{-18}$	17.9	−0.47
Magnesite			9.8	$4.57E^{-10}$	23.5	$4.17E^{-7}$	14.4	1			
Muscovite		25.10	9.8	$1.66E^{-13}$	35	$1.05E^{-11}$	23.6	0.34	$3.02E^{-17}$	58.9	−0.4
Oligoclase			9.8	$1.45E^{-12}$	69.8	$2.14E^{-10}$	65	0.457			
Pyrite			12.9	$2.82E^{-5}$	56.9	$3.02E^{-8}$	56.9	−0.5			
Quarz	19.14		9.8	$1.02E^{-14}$	87.7						
Siderite		1.10	9.8	$1.26E^{-9}$	62.76	$6.46E^{-4}$	36.1	0.5			
Smectite-Ca			151.6	$1.66E^{-13}$	35	$1.05E^{-11}$	23.6	0.34	$3.02E^{-17}$	58.9	−0.4
Smectite-Na			151.6	$1.66E^{-13}$	35	$1.05E^{-11}$	23.6	0.34	$3.02E^{-17}$	58.9	−0.4

A, reactive surface area; k_{25}, kinetic constant at 25 °C; E_a, activation energy; n(H) and n(OH), power term in the calculation of the kinetic rate constant due to acid and base mechanisms, respectively.

[a] Mineralogy of the Aberdeen Ground Formation (Stoker and Bent, 1987) and assumed mineralogy for the Witch Ground, Coal Pit, and Ling Bank Formations. Depth interval between 0–380 mbsf.

[b] Mineralogy of the Norland Shale Group (Audigane et al., 2007). Depth interval between 380–500 mbsf.

[c] See Xu et al. (2006) for the expressions of kinetic rate law and values for the kinetic rate constants. For pyrite, the neutral mechanism has an $n(O_2(aq)) = 0.5$ and the acid mechanism has another species involved $n(O_2(Fe^{3+})) = 0.5$.

Table 4
Initial dissolved component concentrations for a typical sea water with 3.5% salinity (e.g., Turekian, 1968).

Chemical Components	Initial water [mol kg^{-1}] at 15 °C and 1 MPa
Ca^{2+}	1.03×10^{-2}
Mg^{2+}	5.28×10^{-3}
Na^{+}	4.69×10^{-1}
K^{+}	1.02×10^{-2}
HCO_3^{1-}	2.30×10^{-3}
SO_4^{2-}	2.82×10^{-2}
Cl^{1-}	5.46×10^{-1}
Br^{1-}	8.41×10^{-4}
F^{1-}	6.80×10^{-5}
Sr^{2+}	9.10×10^{-5}
CO_2(l)	2.92×10^{-5}
pH	7.89

injected CO_2 is transferred to the ocean during the 100 yrs of our simulation.

To estimate the fracture volumetric fractions and apertures able to increase the cap rock matrix vertical permeability from $10^{-16}\,m^2$ to $10^{-14}\,m^2$ within the chimney, we apply the self-consistent approach (Eqs. 1a, 1b). This is an effective medium model that depends on: (i) the properties of the individual components of the composite medium, (ii) the volumetric fractions of the components, and (iii) the shapes of the components (Mavko et al., 2009). This model treats all components, in our case matrix pores and fractures equally, i.e. it does not required to impose which are the background components and inclusions. To apply the self-consistent approach, let us assume matrix pores with spherical shapes and fractures with disk or needle shapes (Berryman, 1995), and the cubic law (e.g, Witherspoon et al., 1980; Eq. 1c) to estimate the fracture permeability. The cubic law assumes non-cemented, parallel fractures, and estimates fracture permeability depending on fracture aperture and separation.

For a generic chimney, we show calculated chimney effective permeabilities for fracture apertures ranging from 1 to 1000 μm, fracture volumetric fractions from 0 to 2% (or equivalently pore volumetric fractions from 100 to 98%), separations given by Eq. (1d), a chimney radius of 100 m, and a cap rock matrix (pores) permeability of $10^{-16}\,m^2$ (Fig. 4a). The values for the chimney radius and cap rock matrix (pores) permeability are the same as those used in the numerical simulations. Fig. 4a indicates that to increase the vertical permeability in the chimney within the cap rock from $10^{-16}\,m^2$ to values above $10^{-14}\,m^2$, the chimney requires containing vertical fractures with disk apertures larger than 0.05 mm for volume fractions below 1%. This also indicates that high vertical anisotropy permeability ratios (up to about three orders of magnitude) can be expected in chimneys if the pre-existing vertical fractures within it mainly contribute to the vertical flow. Differences in effective permeability if considering disks or needle shapes for the fractures are small (Fig. 4b).

$$f_m(k_m - k^*)X_{spherical} + (1 - f_m)(k_f - k^*)X_{disk,\,needle} = 0; \tag{1a}$$

$$X_{spherical} = \frac{1}{k_m + 2k^*};$$
$$X_{disk} = \frac{1}{9}\left(\frac{1}{k_f} + \frac{2}{k^*}\right);$$
$$X_{needle} = \frac{1}{9}\left(\frac{1}{k^*} + \frac{4}{k_f + k^*}\right); \tag{1b}$$

$$k_f = \frac{a^3}{12s}; \tag{1c}$$

$$s = \frac{a \bullet f_m \bullet r}{r(1 - f_m) - a} \text{ where } s \text{ is only valid for } s < r; \tag{1d}$$

In Eq. (1), f_m is the volume fraction of the matrix pores, k_m, k_f and k^* are the matrix, fracture and effective permeabilities, respectively, r is the radius of the chimney or volume of the chimney per unit of cross sectional area, and a and s are the fracture aperture and separation,

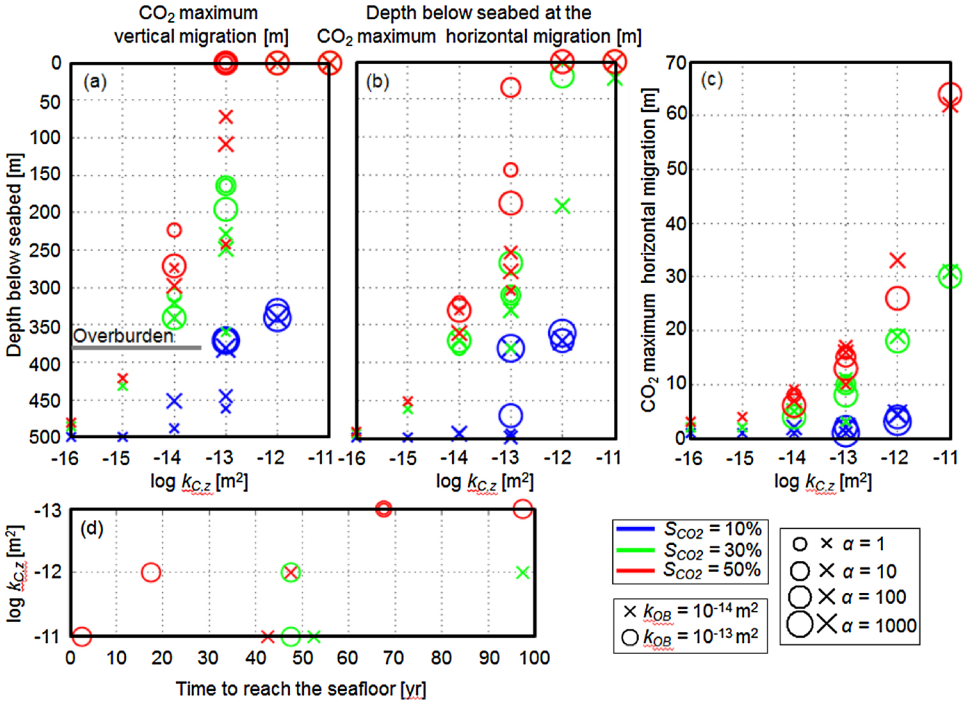

Fig. 3. Summary of the 46 reactive transport simulations after 100 yr with the CO_2 injection point located at 500 m beneath the seabed. Results are shown for injected CO_2 saturations (S_{CO2}) of 10%, 30%, and 50%, overburden matrix permeabilities (k_{OB}) of 10^{-14} m^2 and 10^{-13} m^2, chimney vertical permeabilities ($k_{C,z}$) from 10^{-16} m^2 to 10^{-11} m^2, and ratios between chimney vertical and horizontal permeabilities ($\alpha = k_{C,z}/k_{C,x}$) of 1 to 1000. Note that in (a) the markers for the simulations with S_{CO2} of 30% and 50%, and $k_{C,z}$ of 10^{-12} m^2 and 10^{-11} m^2, simulations where the CO_2 reaches the seabed, overlap. In (c) the results are shown as horizontal distance from the injection point.

respectively.

We describe the main CO_2-induced physicochemical changes for the simulation that uses an injected CO_2 saturation of 50%, overburden matrix permeability of 10^{-13} m^2, and chimney vertical and horizontal permeabilities of 10^{-13} m^2 and 10^{-15} m^2, respectively (Figs. 5–7). We focus on this case because it illustrates that the CO_2 can migrate to the seabed in less than 100 yr with a sensible combination of intrinsic permeabilities. However, we note this simulation, arguably, uses a high CO_2 saturation for chimneys located quite far away from a CO_2 injection well. Higher injected CO_2 saturations increase the CO_2 ascent velocity because there is more CO_2 on the system to overcome its critical saturation, and the CO_2 relative permeability can reach larger values. In our simulations, the bottleneck for the ascent of CO_2 is the time it takes to reach the critical saturation threshold. Let us use the term effective velocities to refer to the ascent velocities that include the time it takes to reach the critical CO_2 saturation. The effective CO_2 ascent velocities in the chimney are about 0.1 m day^{-1}, and once the 0.05% CO_2 saturation threshold is reached the ascent velocities are about 1 m day^{-1}. Effective CO_2 ascent velocities within the chimney of about 0.1 m day^{-1} are consistent with fluid flow rates ranging from 0.03 to 3 m day^{-1} within fault zones (IEAGHG, 2011). The increase in permeability anisotropy ratio in the chimney ($\alpha = k_{C,z}/k_{C,x}$) increases the vertical ascent of CO_2 (e.g., see blue markers in Fig. 3a). Similarly, the effective

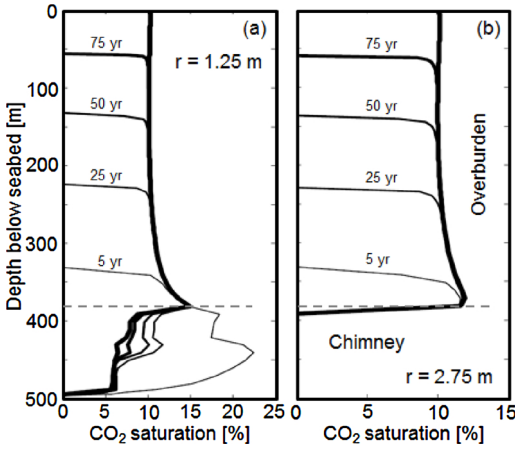

Fig. 5. Temporal evolution over 100 yr of CO_2 saturation with depth at radial distances from the injection point of (a) 1.25 m and (b) 2.75 m. Time steps at 5, 25, 50, 75, and 100 yr for a injected CO_2 saturation of 50%, overburden matrix permeability of 10^{-13} m^2, and chimney vertical and horizontal permeabilities of 10^{-13} m^2 and 10^{-15} m^2.

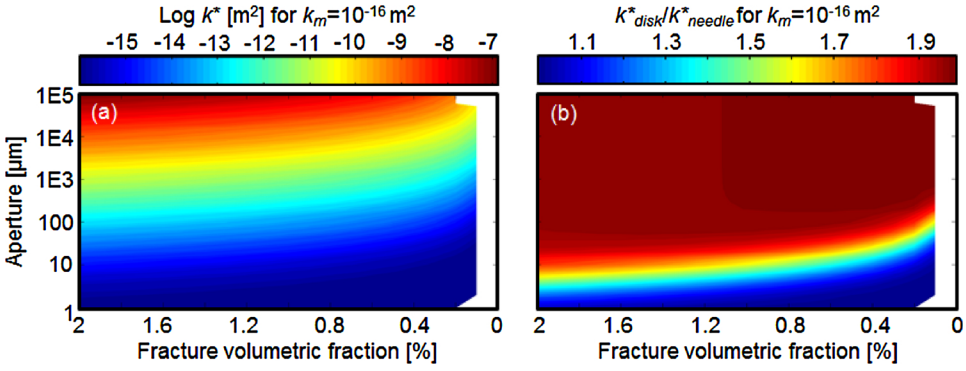

Fig. 4. Variation of the effective permeability of a media composed by pores and fractures with changes in aperture and volumetric fraction of fractures. (a) Effective permeability of a media with spherical (matrix pores) and disk (fractures) shapes calculated with the self-consistent approach (Berryman, 1995) using a matrix permeability of 10^{-16} m^2. (b) Ratio between effective permeabilities calculated with disks and needle shapes for the fractures. The white areas indicate combinations of aperture and matrix volumetric fractions giving non-physically admissible effective permeabilities.

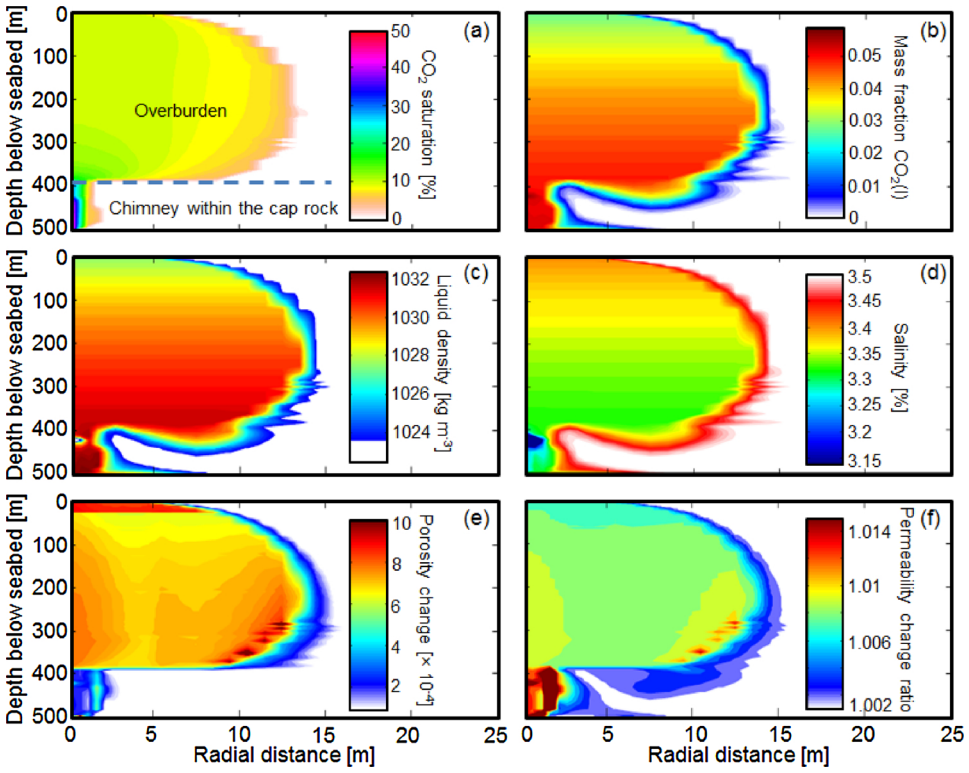

Fig. 6. Example simulation showing the variation of physicochemical properties with depth and radial distance. Simulation results with an injected CO_2 saturation of 50%, overburden matrix permeability of $10^{-13}\,m^2$ and chimney vertical and horizontal permeabilities of $10^{-13}\,m^2$, and $10^{-15}\,m^2$.

ascent velocity at the chimney ($\alpha = 100$) of 0.1 m day^{-1}, is an order of magnitude higher than that in the overburden ($\alpha = 1$) of 0.01 m day^{-1}, for a constant vertical permeability in both geological domains of $10^{-13}\,m^2$ (Fig. 5).

This analysis demonstrates that, for the same volumetric fraction of fractures, chimneys comprising a set of connected vertical fractures are more likely to be a higher risk of CO_2 leakage to the seabed than chimneys with different sets of fracture orientations. The concept is that the more fracture orientations exist in a system, the more isotropic the system tends to behave and less dominant is a particular orientation. However, if different sets of fracture orientations are constrained within the vertical fractures and contribute to increase their connectivity, the risk of CO_2 leakage to the seabed increases. Generally, our results show that the vertical distance from the injection point at which the maximum horizontal CO_2 migration occurs, increases with increasing permeability and CO_2 saturation (Fig. 3b, c). Different CO_2 distributions may originate depending on these parameters, permeability anisotropy within the chimney, contrast between the permeability in the chimney and outside, and level of interlayering. Inverted cone shape-type CO_2 distributions can then be expected in relative homogenous media with

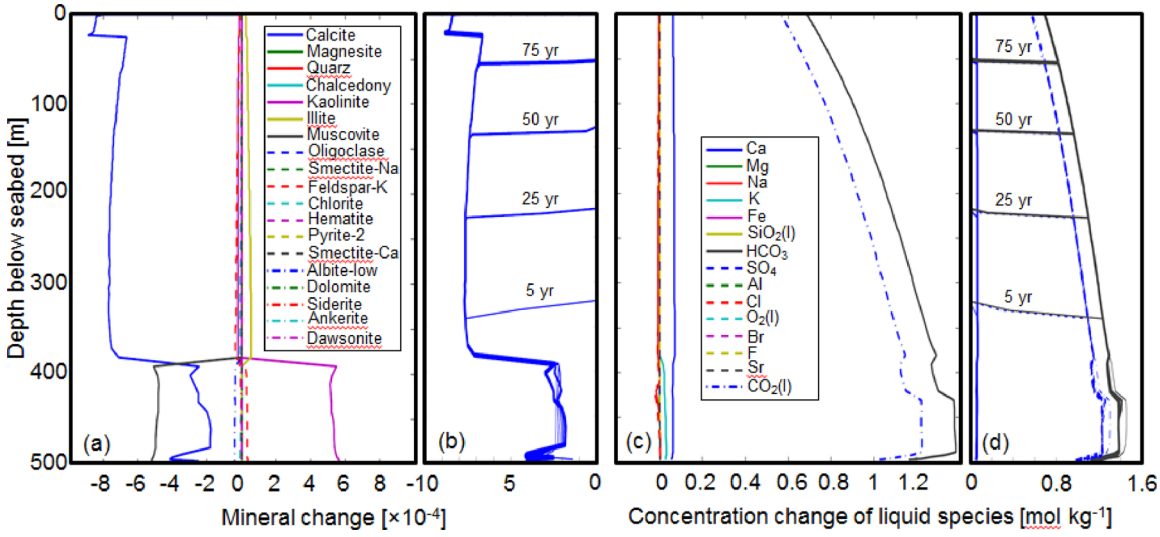

Fig. 7. Depth profiles of changes in (a, b) mineralogy and (c, d) concentration of liquid species at 1.25 m distance from the injection point. (a, c) Results at 100 yr and (b, d) time evolution at 5, 25, 50, 75, and 100 yr of (b) calcite and (d) dissolved CO_2, HCO_3 and Ca. Results for the simulation with injected CO_2 saturation of 50%, overburden matrix permeability of $10^{-13}\,m^2$, and chimney vertical and horizontal permeabilities of $10^{-13}\,m^2$ and $10^{-15}\,m^2$. In (a, b) negative values indicate dissolution and positive precipitation. In (c, d) positive values indicate increase in concentration of liquid species.

high permeability, high CO_2 saturations; less well-defined distributions, otherwise (Fig. 6a).

An increase in the mass fraction of dissolved CO_2 slightly increases the liquid phase density and decreases the salinity (Fig. 6b–d). Although the increase in density due to dissolved CO_2 is small, in this case less than 1%, it can generate density driven flow and enhance dissolution of CO_2 by advective mixing. In particular, this can happen during periods where the CO_2 input to the chimney is low, and the CO_2 rich water within the two phase zone may migrate downwards and be replaced with water with less dissolved CO_2.

In our simulations salt does not precipitate, and the modest decrease in salinity within the two phase zone is caused by the slight increase in total mass of liquid phase upon CO_2 dissolution. After 100 yr of injection, changes in porosity due to mineral precipitation/dissolution and associated changes in permeability are very small (Fig. 6e, f). These small changes are primarily related to calcite dissolution (Fig. 7a, b), triggered by dissolved CO_2 in the formation water, causing a pH drop from an initial value of 7.89 to values between 5.0 to 5.4 and increasing the concentration of calcium ions [Ca^{2+}] (Fig. 7c, d). The increase in bicarbonate ions [HCO_3^{1-}] (Fig. 7c, d) originates from (i) the increase in carbonic acid [H_2CO_3] in the formation water that dissociates rapidly into bicarbonate ion [HCO_3^{1-}] and hydrogen ions [H^+], and (ii) the reaction of these [H^+] with the produced carbonate ions [CO_3^{2-}] from the dissolution of calcite. The dissolved carbonate ions can also react with dissolved calcium ions to re-precipitate calcite (e.g., Audigane et al., 2007), but this is not observed in our 100 yr simulations.

4. Discussion

Our focus is on the risk of chimneys acting as conduits for CO_2 leakage at the seabed over the time scale of CO_2 injection activity (here conservatively assumed to be 100 yr), and not on the longer term storage of CO_2. Over a 100 yr, our results indicate that the risk of CO_2 leakage to the seabed through chimneys is primarily controlled by the pre-existing hydrogeological state of the system, into which the CO_2 is injected, and not by chemically related changes in the system's porosity (increase of less than 0.1% and 0.25% in the cap rock and overburden, respectively) and permeability (increase of less than 1.4% and 1% in the cap rock and overburden, respectively). For the mineralogy considered, this time window is not sufficient for CO_2 related mineral precipitation/dissolution to affect the ascent of CO_2 within the chimney. This modelling insight also applies to fluid escape structures found in many other sedimentary basins (e.g., Cartwright and Santamarina, 2015) with similar carbonate content (10 to 20% of solid volume) and pH of the formation water (about 7.8; pH normal seawater). CO_2-induced carbonate dissolution dominates the chemical response, very slightly increasing the porosity and permeability of the cap rock and overburden. Some experimental results show that calcite dissolution can have the opposite effect, and decrease fracture permeability by mobilization of less soluble mineral particles (e.g., Ellis et al., 2013). Note that we do not consider mineral dissolution-induced mechanical weakening and compaction (e.g., Roded et al., 2018; Vialle and Vanorio, 2011) that could reduce porosity and permeability over short time periods; this effect can be small depending on the mineralogy (e.g., Hangx et al., 2013). Neither do we consider CO_2 injection induced hydro-fracturing, but this mechanism is likely secondary in chimneys experiencing CO_2 flow rates incapable of generating large overpressures; particularly for scenarios sufficiently far away from the injection point.

Audigane et al. (2007), whose mineralogy we use, present reactive transport simulations of CO_2 injection and long term storage at the Sleipner Site, North Sea. Before the CO_2 injection simulations, they performed a chemical equilibrium of the formation water with the minerals for 10,000 yr which results in a pH of 7.67, similar to the pH of 7.89 of our assumed typical sea water with 3.5% salinity. During the 25 yr of CO_2 injection, their simulations also indicate very minor induced porosity changes (less 1%). Over long time periods (10,000 yr), their results show mineral dissolution in the cap rock (increase in porosity from 0.125 to 0.144) and precipitation in the overburden (decrease in porosity from 0.42 to 0.40). Although, longer time periods may increase mineral dissolution within the chimney, the associated porosity and permeability increase reported by Audigane's et al. (2007) is not high enough to substantially affect the hydrodynamic response of the system. However, the long period response could be the worst case scenario for CO_2 leakage through chimneys, if CO_2 induced mineral precipitation, including salt precipitation, is sufficient to push the matrix grains apart and/or develop fractures (e.g., Scherer, 1999), as has been observed experimentally for halite precipitation (e.g., Noiriel et al., 2010).

We assumed grid block scale effective reaction rate constants, porosity and permeability, and did not explicitly model a double porosity, double permeability interacting continua (e.g., Xu et al., 2006), because: (i) our lack of in-situ data constraints on geometric fracture parameters such as aperture, separation, connectivity and length, and (ii) the current limited precise knowledge on the processes controlling the pore size range over which precipitation occurs (Stack et al., 2014). If mineral precipitation/dissolution localizes in the fractures within the chimney, because it is inhibited in smaller pores (e.g., Emmanuel et al., 2010), even small changes in mineral content may create significant changes in fracture permeability, and so in the ascent of CO_2, and our results may underestimate this effect. However, there is a lack of consensus in the literature for the pore-size dependence of precipitation/dissolution as it may occur over all pore sizes with no intrinsic pore-size dependence, preferentially in smaller pores, or in different pores depending on the system's chemistry (Stack et al., 2014 and references therein). We overcome the pore size dependence on precipitation/dissolution affecting permeability by using the "Tube in Series" model (Verma and Pruess, 1988), which considers a bundle of large pores connected to smaller pores in series. This model assumes precipitation by uniform solid grain coating and so the pore throats become filled leaving the largest pore spaces open. As a result, the permeability of the formation is reduced, as the connectivity between difference size pores is blocked.

In our simulations, we assumed hydrostatic conditions at the injection point and so CO_2 flow through the chimney is driven by buoyancy. Our simulated generic chimney is located sufficiently far away from a hypothetical CO_2 injection well and so, when the CO_2 reaches it, the potential overpressure generated close to the injection well has likely dissipated. Furthermore, it contains pre-existing sub-vertical fractures and so its formation fluids are not likely overpressured. CO_2 migrates 500 m or more vertically (reaches the seabed) in less than 100 yr with injected CO_2 saturations at or above 30%, a critical gas saturation of 5%, and chimney vertical permeabilities and overburden isotropic permeabilities both above $10^{-14}\,m^2$. Karstens et al. (2017) present numerical fluid flow simulations to assess the leakage potential of chimneys located at 7 km from the injection point at the Sleipner site, North Sea. Similarly, they conclude that if the CO_2 plume reaches a chimney, then a chimney vertical permeability of $10^{-14}\,m^2$ may be sufficient for CO_2 leakage at the seabed to occur. To increase the vertical permeability in the chimney within the cap rock from $10^{-16}\,m^2$ to values above $10^{-14}\,m^2$, the chimney requires vertical fractures with apertures larger than 0.05 mm for volume fractions below 1%. Hence, only if high CO_2 saturations reach a pre-existing chimney containing relatively small fracture apertures and sensible fracture volumetric fractions, is there a potential risk of CO_2 leakage at the seabed over the time scale of CO_2 injection activities.

Our insights have some important caveats. Here we have likely assessed a high-risk CO_2 leakage scenario by assuming: (i) that the chimney terminates at the top of the cap rock, (ii) a relatively high cap rock permeability of $10^{-16}\,m^2$, (iii) open fractures, (iv) a constant supply of CO_2 over the whole duration of the simulations, and (v) a critical CO_2 saturation of 5%. If the chimney did not reach the top of the

cap rock, the risk would considerably diminish. In contrast, if the chimney penetrated the overburden this would have a minor impact because the vertical permeabilities of the chimney that produce CO_2 leakage at the seabed in less than 100 yr, are the same order of magnitude, above 10^{-14} m^2, as typical overburden vertical permeabilities. Cap rock permeabilities in similar systems can be as low as about 10^{-20} m^2, and so if a chimney existed in a cap rock with lower permeabilitity it would need to contain considerably larger fracture apertures to be a risk. Relatively shallow chimneys can be active (e.g., Bull et al., 2018a,b) and so it is sensible to assume that some fractures within them are open. If the fractures were closed, the effective permeability of the chimney would be similar to that of the cap rock matrix/pores, and so the risk of CO_2 leakage at the seabed would be very small. A constant supply of CO_2 reduces the relative contribution of imbibition, displacement of the non-wetting fluid (CO_2) by the wetting fluid (brine). In natural systems, however, a discontinuous supply of CO_2 to the chimney may occur increasing the relative contribution of imbibition and retarding the CO_2 ascent to the seabed. The effective CO_2 ascent velocity is particularly controlled by the critical CO_2 saturation parameter. This parameter can range from 0 to 38% (Skauge et al., 1999). The closer the CO_2 saturation value is to its critical threshold, the lower are the relative permeability to CO_2, the effective CO_2 ascent velocity, and the risk of CO_2 leakage at the seabed.

5. Concluding remarks

Over the time scale of the CO_2 injection activity our simulations indicate:

(i) Only if high CO_2 saturations (at or above 30%) reach a chimney in the cap rock with an effective vertical permeability above 10^{-14} m^2, caused by pre-existing sub-vertical fractures with minimum apertures of 0.05 mm and volumetric fractions below 1% within it, is there a risk of CO_2 leakage at the seabed. In practice, a site for CO_2 storage is unlikely to be selected where a large chimney structure imaged on seismic reflection data is likely to act as a seal bypass system over a significant proportion of the sedimentary overburden.

(ii) CO_2-induced mineral precipitation/dissolution within chimneys, and associated changes in porosity and permeability, are very small.

(iii) The pre-existing hydrogeological state of marine systems with a carbonate solid content of about 10–20% and formation water pH similar to that of normal sea-water of 7.8, primarily controls the risk of CO_2 leakage at the seabed through chimneys located sufficiently far away from the injection point.

To fully understand and better assess the degree to which chimneys facilitate the transport of CO_2, and other greenhouse gases such as CH_4, to the seabed, extensive in-situ geological, geophysical, and geochemical data constraints and reactive transport laboratory experiments in samples with fractures are needed. In particular, high resolution broadband seismic experiments in combination with sophisticated rock physics models, to constrain geometric fracture parameters such as aperture, separation, connectivity and length (e.g., Bull et al., 2018a,b), and laboratory measurements of the critical gas saturation threshold in fracture media, are essential.

Acknowledgements

This work was supported by the Natural Environment Research Council [CHIMNEY; NERC Highlight Topic; NE/N016130/1]. We thank Lawrence Berkeley National Laboratory for the online open manuals of TOUGHREACT v3 (http://esd1.lbl.gov/FILES/research/projects/tough/documentation/TOUGHREACT_V3-OMP_RefManual.pdf), ECO2 (http://esd1.lbl.gov/files/research/projects/tough/documentation/TOUGH2_V2_Users_Guide.pdf). We thank Eric Sonnenthal at Lawrence Berkeley National Laboratory for his advice during the set-up of the TOUGHREACT v3.32 simulations. We also thank Joe Cartwright and an anonymous reviewer for their thorough and constructive comments.

Appendix A. Fluid flow related assumptions, their justification and evaluation

Table A1
Summary of major fluid flow related assumptions in our simulations, and their justification and evaluation. For a more detailed discussion about these assumptions and their impact refer to the main text.

Assumption	Justification	Evaluation
Effective homogenous media to approximate the fluid flow contribution from both fracture and porous flows in the chimney.	Commonly applied concept to model macro-scale fluid flow processes in geological systems containing closely spaced pre-exiting fractures.	Interactions between pore and fracture flows are not simulated. The validity of this assumption decreases with the decrease in pre-existing fracture density and increase in fracture aperture.
Chimney containing parallel, open fractures that are not connected at different orientations and, that only contribute to the flow in the direction they are aligned with.	Simplest conceptual model in the absence of sufficient data to constrain a more complex model. Observations from natural systems indicating that chimneys can be active pathways for natural gas to reach the seabed	The time estimated for the CO_2 to reach the seabed could be either (i) an optimistic estimate because fracture orientations constrained within the vertical fractures cannot contribute to increase their connectivity and vertical flow or (ii) a conservative estimate because fractures could be closed.
Hydrostatic pressure conditions within and outside the chimney	Chimney located sufficiently far away from the injection point allowing near well injection-induced overpressure to dissipate. Chimney containing pre-existing open fractures reducing the likelihood of overpressured formation fluids.	CO_2 flow driven by buoyancy.
Chimney terminating at the top of the cap rock.	The cap rock is the bottleneck to the ascent of CO_2. The overburden has much higher matrix vertical permeabilities than those of the cap rock. Pre-existing factures within the chimney are likely to be closed in relatively high porosity, low stiffness overburden sediments	The time estimated for the CO_2 to reach the seabed is a conservative estimate. Longer times would occur if the chimney does not reach the top of the cap rock

(*continued on next page*)

Table A1 (*continued*)

Assumption	Justification	Evaluation
Overburden isotropic permeabilities of 10^{-13} and 10^{-14} m^2.	Commonly used/measured permeabilities for overburden sediments at depths of a few hundred meters below the seabed	Overburden permeabilities similar to chimney effective vertical permeabilities. Isotropic permeabilities in the overburden limit the lateral migration of CO_2 and its accumulation at several 10 s of metres below the seabed.
Cap rock matrix isotropic permeability of 10^{-16} m^2.	Cap rock permeability within the range of cap rock permeabilities found in the literature and used in other numerical modelling studies of CO_2 injection	Lower matrix cap rock permeabilities from 10^{-19} to 10^{-21} m^2 are also reported at relevant CO_2 storage sites. Chimneys formed in lower cap-rock permeabilities would need considerably larger fracture apertures to be a risk of CO_2 leakage at the seabed.
Chimney vertical permeabilities from 10^{-16} to 10^{-11} m^2.	Sensible volumetric fractions and relatively small apertures of closely spaced sub-vertical pre-existing fractures can generate such high vertical permeabilities.	Lateral CO_2 migration within the chimney in the cap rock is very limited due to the high vertical anisotropy ratio.
Constant CO_2 injection over the whole duration of the simulations.	A fully developed CO_2 pathway or plume can supply a constant mass of CO_2 to a potential chimney located within it.	A discontinuous supply of CO_2 would increase the relative contribution of imbibition and retard the CO_2 ascent to the seabed.
CO_2 saturations of 10%, 30%, and 50%.	In natural CO_2 storage reservoirs, such as Sleipner, North Sea, CO_2 saturations above 30% have been estimated several hundreds of meters away from the injection well a few years after injection starts.	CO_2 saturations above 50% would generate greater CO_2 ascent velocities within the chimney and reduce the time estimated for the CO_2 to reach the seabed. Lower saturations than 10% would considerably reduce the ascent velocity because they would be closer to the CO_2 critical saturation threshold.
Critical CO_2 saturation of 5%.	Commonly used value in similar CO_2 injection numerical modelling studies. Critical gas saturations from 0% to 38% have been reported in the literature.	The time estimated for the CO_2 to reach the seabed could be longer/shorter if this value increases/decreases.

Appendix B. Supplementary data

Supplementary material related to this article can be found, in the online version, at doi:https://doi.org/10.1016/j.ijggc.2019.04.018.

References

Ahmad, N., Wörman, A., Sanchez-Vila, X., Bottacin-Busolin, A., 2016. The role of advection and dispersion in the rock matrix on the transport of leaking CO2-saturated brine along a fractured zone. Adv. Water Resour. 98, 132–146. https://doi.org/10.1016/j.advwatres.2016.10.006.

Arntsen, B., Wensaas, L., Løseth, H., Hermanrud, C., 2007. Seismic modeling of gas chimneys. Geophysics 72, SM251–SM259. https://doi.org/10.1190/1.2749570.

Audigane, P., Gaus, I., Czernichowski-Lauriol, I., Pruess, K., Xu, T., 2007. Two-dimensional reactive transport modeling of CO2 injection in a saline aquifer at the Sleipner site, North Sea. Am. J. Sci. 307, 974–1008. https://doi.org/10.2475/07.2007.02.

Berndt, C., 2005. Focused fluid flow in passive continental margins. Philos. Trans. Math. Phys. Eng. Sci. 363, 2855–2871. https://doi.org/10.1098/rsta.2005.1666.

Berryman, J., 1995. Mixture theories for Rock properties. In: Ahrens, T.J. (Ed.), Rock Physics and Phase Relations: a Handbook of Physical Constants. American Geophysical Union, Washington, pp. 205–228. https://doi.org/10.1029/RF003p0205.

Bull, J., et al., 2018a. Cruise Report RRS James Cook 152 - JC152: CHIMNEY - Characterisation of Major Overburden Pathways Above Sub-seafloor CO2 Storage Reservoirs in the North Sea. Scanner and Challenger Pockmark Complexes, 55 pp., University of Southampton, UK. . https://eprints.soton.ac.uk/420257.

Bull, J., et al., 2018b. Constraining the physical properties of chimney/pipe structures within sedimentary basins. 14th International Conference on Greenhouse Gas Control Technologies, GHGT-14.

Bünz, S., Mienert, J., Berndt, C., 2003. Geological controls on the Storegga gas-hydrate system of the mid-Norwegian continental margin. Earth Planet. Sci. Lett. 209, 291–307. https://doi.org/10.1016/S0012-821X(03)00097-9.

Cartwright, J., Santamarina, C., 2015. Seismic characteristics of fluid escape pipes in sedimentary basins: implications for pipe genesis. Mar. Pet. Geol. 65, 126–140. https://doi.org/10.1016/j.marpetgeo.2015.03.023.

Cartwright, J., Huuse, M., Aplin, A., 2007. Seal bypass systems. Bull. 91, 1141–1166. https://doi.org/10.1306/04090705181.

Cavanagh, A.J., Haszeldine, R.S., 2014. The Sleipner storage site: Capillary flow modeling of a layered CO2 plume requires fractured shale barriers within the Utsira Formation. Int. J. Greenh. Gas Control. 21, 101–112. https://doi.org/10.1016/j.ijggc.2013.11.017.

Chadwick, R.A., Noy, D.J., 2015. Underground CO2 storage: demonstrating regulatory conformance by convergence of history-matched modeled and observed CO2 plume behavior using Sleipner time-lapse seismics. Greenh. Gases Sci. Technol. 5, 305–322. https://doi.org/10.1002/ghg.1488.

Chadwick, R.A., Arts, R., Eiken, O., 2005. 4D seismic quantification of a growing CO2 plume at sleipner, North Sea. Geological Society, London, Petroleum Geology Conference Series 6 1385–1399. https://doi.org/10.1144/0061385.

Corey, A.T., 1954. The interrelation between gas and oil relative permeabilities. Producers Monthly 19 (November), 38–41.

Dentzer, J., Bruel, D., Delescluse, M., Chamot-Rooke, N., Beccaletto, L., Lopez, S., Courrioux, G., Violette, S., 2018. Thermal and seismic hints for chimney type cross-strata fluid flow in onshore basins. Sci. Rep. 8, 15330. https://doi.org/10.1038/s41598-018-33581-x.

Ellis, B.R., Fitts, J.P., Bromhal, G.S., McIntyre, D.L., Tappero, R., Peters, C.A., 2013. Dissolution-driven permeability reduction of a fractured carbonate caprock. Environ. Eng. Sci. 30, 187–193. https://doi.org/10.1089/ees.2012.0337.

Emmanuel, S., Ague, J.J., Walderhaug, O., 2010. Interfacial energy effects and the evolution of pore size distributions during quartz precipitation in sandstone. Geochim. Cosmochim. Acta 74, 3539–3552. https://doi.org/10.1016/j.gca.2010.03.019.

Espinoza, D.N., Santamarina, J.C., 2017. CO2 breakthrough—Caprock sealing efficiency and integrity for carbon geological storage. Int. J. Greenh. Gas Control. 66, 218–229. https://doi.org/10.1016/j.ijggc.2017.09.019.

Gafeira, J., Long, D., 2015. Geological Investigation of Pockmarks in the Scanner Pockmark SCI Area, JNCC Report 571. JNCC, Peterborough 2015.

Hangx, S., van der Linden, A., Marcelis, F., Bauer, A., 2013. The effect of CO_2 on the mechanical properties of the Captain Sandstone: geological storage of CO_2 at the Goldeneye field (UK). Int. J. Greenh. Gas Control. 19, 609–619. https://doi.org/10.1016/j.ijggc.2012.12.016.

Harper, M.L., 1971. Approximate geothermal gradients in the North Sea Basin. Nature 230, 235–236. https://doi.org/10.1038/230235a0.

Hustoft, S., Bünz, S., Mienert, J., 2010. Three-dimensional seismic analysis of the morphology and spatial distribution of chimneys beneath the Nyegga pockmark field, offshore mid-Norway. Basin Res. 22, 465–480. https://doi.org/10.1111/j.1365-2117.2010.00486.x.

IEAGHG, 2011. Caprock Systems for CO_2 Geological Storage. International Energy Agency Report: 2001/01, May 2011.

Judd, A., Long, D., Sankey, M., 1994. Pockmark formation and activity, U.K. Block 15/25, North Sea. Bull. Geol. Soc. Denmark 41, 34–49.

Karstens, J., Berndt, C., 2015. Seismic chimneys in the Southern Viking Graben – implications for palaeo fluid migration and overpressure evolution. Earth Planet. Sci. Lett. 412, 88–100. https://doi.org/10.1016/j.epsl.2014.12.017.

Karstens, J., Ahmed, W., Berndt, C., Class, H., 2017. Focused fluid flow and the subseabed storage of CO2: evaluating the leakage potential of seismic chimney structures for the Sleipner CO2 storage operation. Mar. Pet. Geol. 88, 81–93. https://doi.org/10.1016/j.marpetgeo.2017.08.003.

Løseth, H., Gading, M., Wensaas, L., 2009. Hydrocarbon leakage interpreted on seismic data. Mar. Pet. Geol. 26, 1304–1319. https://doi.org/10.1016/j.marpetgeo.2008.09.008.

Mavko, G., Mukerji, T., Dvorkin, J., 2009. The Rock Physics Handbook, 2nd ed. Cambridge University Press, New York.

Mbia, E.N., Frykman, P., Nielsen, C.M., Fabricius, I.L., Pickup, G.E., Bernstone, C., 2014. Caprock compressibility and permeability and the consequences for pressure development in CO2 storage sites. Int. J. Greenh. Gas Control. 22, 139–153. https://doi.

org/10.1016/j.ijggc.2013.12.024.
Narasimhan, T.N., Witherspoon, P.A., 1976. An integrated finite difference method for analyzing fluid flow in porous media. Water Resour. Res. 12, 57–64. https://doi.org/10.1029/WR012i001p00057.
Noiriel, C., Renard, F., Doan, M.-L., Gratier, J.-P., 2010. Intense fracturing and fracture sealing induced by mineral growth in porous rocks. Chem. Geol. 269, 197–209. https://doi.org/10.1016/j.chemgeo.2009.09.018.
Paul, M.A., Jobson, L.M., 1991. Geotechnical Properties of Soft Clays from the Witch Ground Basin, Central North Sea, vol. 7. Geological Society, London, Engineering Geology Special Publications, pp. 151–156. https://doi.org/10.1144/gsl.eng.1991.007.01.12.
Preisig, M., Prévost, J.H., 2011. Coupled multi-phase thermo-poromechanical effects. Case study: CO2 injection at In Salah, Algeria. Int. J. Greenh. Gas Control. 5, 1055–1064. https://doi.org/10.1016/j.ijggc.2010.12.006.
Pruess, K., 2005. ECO2N: A TOUGH2 Fluid Property Module for Mixtures of Water, NaCl and CO2, Report LBNL-57952. Lawrence Berkeley National Laboratory, Berkeley, Calif.
Pruess, K., Müller, N., 2009. Formation dry-out from CO2 injection into saline aquifers: 1. Effects of solids precipitation and their mitigation. Water Resour. Res. 45. https://doi.org/10.1029/2008WR007101.
Roded, R., Paredes, X., Holtzman, R., 2018. Reactive transport under stress: permeability evolution in deformable porous media. Earth Planet. Sci. Lett. 493, 198–207. https://doi.org/10.1016/j.epsl.2018.04.041.
Rutqvist, J., Birkholzer, J.T., Tsang, C.-F., 2008. Coupled reservoir–geomechanical analysis of the potential for tensile and shear failure associated with CO2 injection in multilayered reservoir–caprock systems. Int. J. Rock Mech. Min. Sci. 45, 132–143. https://doi.org/10.1016/j.ijrmms.2007.04.006.
Scherer, G.W., 1999. Crystallization in pores. Cem. Concr. Res. 29, 1347–1358. https://doi.org/10.1016/S0008-8846(99)00002-2.
Shell UK Limited, 2014. Peterhead CCS Project – Well Completion Concept Select Report. PCCS-05-PT-ZW-7180-00003. .
Skauge, A., Haaskjold, G.S., Ormehaug, P.A., Aarra, M.G., 1999. Studies of production under bubblepoint. EAGE - 10th European Symposium on Improved Oil Recovery. https://doi.org/10.3997/2214-4609.201406340.
Stack, A.G., Fernandez-Martinez, A., Allard, L.F., Bañuelos, J.L., Rother, G., Anovitz, L.M., Cole, D.R., Waychunas, G.A., 2014. Pore-size-dependent calcium carbonate precipitation controlled by surface chemistry. Environ. Sci. Technol. 48, 6177–6183. https://doi.org/10.1021/es405574a.
Stoker, M.S., Bent, A.J.A., 1987. Lower pleistocene deltaic and marine sediments in boreholes from the central North Sea. J. Quat. Sci. 2, 87–96. https://doi.org/10.1002/jqs.3390020202.
Tasianas, A., Martens, I., Bünz, S., Mienert, J., 2016. Mechanisms initiating fluid migration at Snøhvit and Albatross fields, Barents Sea. Arktos 2, 26. https://doi.org/10.1007/s41063-016-0026-z.
Turekian, K., 1968. Oceans. Prentice-Hall, Englewood, Cliffs, N.J.
van Genuchten, M.T., 1980. A closed-form equation for predicting the hydraulic conductivity of unsaturated soils. Soil Sci. Soc. Am. J. 44, 892–898. https://doi.org/10.2136/sssaj1980.03615995004400050002x.
Verma, A., Pruess, K., 1988. Thermohydrological conditions and silica redistribution near high-level nuclear wastes emplaced in saturated geological formations. J. Geophys. Res. Solid Earth 93, 1159–1173. https://doi.org/10.1029/JB093iB02p01159.
Vialle, S., Vanorio, T., 2011. Laboratory measurements of elastic properties of carbonate rocks during injection of reactive CO_2-saturated water. Geophys. Res. Lett. 38. https://doi.org/10.1029/2010GL045606.
Vilarrasa, V., Bolster, D., Olivella, S., Carrera, J., 2010. Coupled hydromechanical modeling of CO2 sequestration in deep saline aquifers. Int. J. Greenh. Gas Control. 4, 910–919. https://doi.org/10.1016/j.ijggc.2010.06.006.
Williams, G.A., Chadwick, R.A., Vosper, H., 2018. Some thoughts on Darcy-type flow simulation for modelling underground CO2 storage, based on the Sleipner CO2 storage operation. Int. J. Greenh. Gas Control. 68, 164–175. https://doi.org/10.1016/j.ijggc.2017.11.010.
Witherspoon, P.A., Wang, J.S.Y., Iwai, K., Gale, J.E., 1980. Validity of cubic law for fluid flow in a deformable rock fracture. Water Resour. Res. 16, 1016–1024. https://doi.org/10.1029/WR016i006p01016.
Wolery, T.J., 1992. EQ3/6, A Software Package for Geochemical Modeling of Aqueous Systems: Package Overview and Installation Guide (Version 7.0), UCRL-MA-110662-Pt.1. Lawrence Livermore National Lab., Livermore, Calif.
Xu, T., Samper, J., Ayora, C., Manzano, M., Custodio, E., 1999. Modeling of non-isothermal multi-component reactive transport in field scale porous media flow systems. J. Hydrol. 214, 144–164. https://doi.org/10.1016/S0022-1694(98)00283-2.
Xu, T., Apps, J.A., Pruess, K., 2003. Reactive geochemical transport simulation to study mineral trapping for CO2 disposal in deep arenaceous formations. J. Geophys. Res. Solid Earth 108. https://doi.org/10.1029/2002JB001979.
Xu, T., Sonnenthal, E., Spycher, N., Pruess, K., 2006. TOUGHREACT—a simulation program for non-isothermal multiphase reactive geochemical transport in variably saturated geologic media: applications to geothermal injectivity and CO2 geological sequestration. Comput. Geosci. 32, 145–165. https://doi.org/10.1016/j.cageo.2005.06.014.
Xu, T., Sonnenthal, E., Spycher, N., Zheng, L., 2017. TOUGHREACT V3.32 Reference Manual: a Parallel Simulation Program for Non-isothermal Multiphase Geochemical Reactive Transport. Lawrence Berkeley National Laboratory, Report LBNL-Draft, Berkeley, Calif.